Supplement of Atmos. Chem. Phys., 26, 12887–12909, 2026
https://doi.org/10.5194/acp-26-12887-2026-supplement

Atmospheric Chemistry and Physics
Open Access

Supplement of

Ice core insights into the morphology and composition of mineral dust deposited in the tropical Peruvian Andes

Austin M. Weber et al.

Correspondence to: Austin M. Weber (weber.1158@osu.edu)

Note from the authors: All references cited herein are cited within the main text of the manuscript.

S1. Mineral Classification

Five independent mineral classification algorithms[1] were applied to the EDS data for each particle analyzed in this study (Table S1). All of these algorithms, with the exception of the Severin dichotomous key, were automated using the open-source MATLAB® functions provided by Weber (2025) at https://github.com/weber1158/eds-classification. The outputs were cross-referenced with one another and with the Severin dichotomous key to determine the most likely mineral for each particle. The limitations presented in the table clarify the importance of relying on more than just one algorithm to determine mineralogy.

Table S1. Details on the mineral classification algorithms used in the text, including relevant classification criteria, benefits, and individual functions.

Algorithm	Algorithm Type	Classification Criteria	Benefits	Limitations
Donarummo et al. (2003)	Sorting scheme	EDS net intensity	Fast algorithm; designed for, and commonly used in, ice core studies	Restricted to aluminosilicate minerals; many “Unknown” classification nodes
Kandler et al. (2011)	Comparative criteria	Atom percent relative abundance	44 mineral groups, including quartz, salts (e.g., NaCl), and mixtures	Mostly broad mineral groups, not necessarily specific minerals
Panta et al. (2023)	Comparative criteria	Atom percent relative abundance	23 mineral classes, including simple minerals such as quartz and calcite	Cannot differentiate plagioclase solid solution or mafic minerals (pyroxene, amphibole, etc.)
Severin (2004)	Dichotomous key	EDS full spectrum	Includes 182 reference mineral spectra; very easy to use	Requires access to information in Severin (2004), usually in the form of a hard copy of the book; qualitative only; can be subjective and cannot be automated
Weber (2025)	Ensemble machine learning classifier	EDS net intensity	Provides probability table; can recognize palygorskite and can differentiate plagioclase solid solution series and is trained to recognize certain mafic minerals (e.g., pyroxenes)	Restricted primarily to aluminosilicate minerals

[1] The term “algorithm” is used here to describe a set of instructions that can be followed manually or with automation.

S2. Coulter Counter (CC) analysis

In the CC data for HC-19A, particle concentrations are binned within 14 discrete size channels ranging from 0.63—0.80 µm to 12.70—16.00 µm (Weber et al., 2026a). This method of evaluating particle sizes is very different from the image processing technique used in our SEM analysis (main text; Section 3.4 and Section 4.1). Although the image processing technique allows for more precise quantification of the shape and size characteristics of individual grains, the advantage of the CC technique is that size distributions can be inferred from a much larger sample size and therefore the CC technique should be considered more representative of the "true" population size distribution.

Using electron microscopy, we show that mineral dust in HC-19A follows a lognormal distribution; however, the CC data are approximately linear when plotted on the log-log scale (Fig. S1), which is consistent with a distribution described by a power-law. This finding is inconsistent with previous ice core microparticle studies that identified lognormal distributions using both CC and SEM (e.g., Royer et al., 1983). However, Groundwater et al. (2012) show that power-law distributions are commonly observed in particle samples and that the CC technique is capable of detecting more particles in the <1 µm size fraction than SEM. Royer et al. (1983) also find that the modal values obtained from CC and SEM measurements can differ by a factor of ~2 (with SEM measurements producing the higher modal values), which is likely because SEM image analyses are two-dimensional and do not account for the thickness of individual particles (and since particles preferentially settle on their largest side, SEM-derived size measurements may be overestimated).

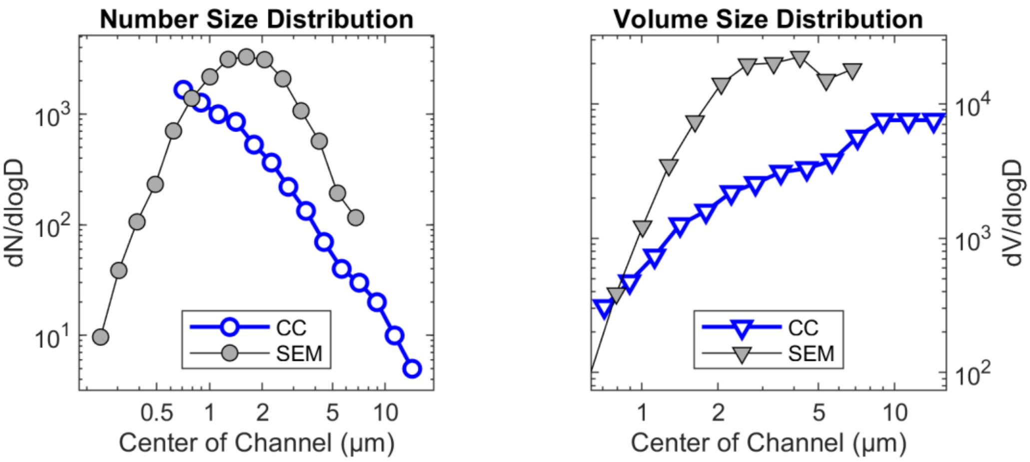

Figure S1. Dust size distributions in HC-19A (1960–2018 CE), as determined by Coulter Counter (CC) and SEM. The CC data are plotted using the median dust concentration from each size channel.

The findings illustrated here are likely explained by a SEM operator bias. Due to the difficulty of collecting well-resolved EDS spectra on very small particles, the number of particles <2 µm analyzed by SEM is underrepresented compared to the "true" distribution measured by the CC technique.

S3. Principal component analysis (PCA)

We find that particle aspect ratio and circularity exhibit a moderate inverse relationship (Spearman $\rho = -0.55$, p-value < 0.001). This is expected because as a particle becomes more elongated it becomes less circular. To account for correlations between our morphological variables, we apply PCA for dimensionality reduction. We focus specifically on the mineral groups with at least 30 observations and standardize the three morphological measurements using z-scores.

The first two principal components (PC1 and PC2) explain 86% of the total variance in the standardized morphological data. The loading coefficients are given in Table S2. Based on these results, PC1 is primarily a shape axis influenced by the inverse relationship between aspect ratio and circularity. Particles with low PC1 scores are elongated and irregular whereas particles with high PC1 scores are more equant and circular. PC2 is predominantly governed by ECD, and so PC2 is interpreted as a size axis. Larger particles exhibit high PC2 scores while smaller particles are represented by low PC2 scores. PC3 is strongly influenced by particle shape, but because it only explains 14% of the total variance we do not interpret PC3 in detail.

Table S2. Loading coefficients for the PCA. **Bold** is used to emphasize significant values.

	PC1 (54%)	PC2 (32%)	PC3 (14%)
log(ECD)	−0.34	**+0.90**	+0.28
Aspect Ratio	**−0.63**	−0.44	**+0.64**
Circularity	**+0.70**	+0.05	**+0.72**

Figure S2 illustrates the PCA results with respect to mineralogy by plotting the centroids of each mineral in the principal component space for PC1 and PC2 along with their 95% confidence ellipses. The biplot shows that all major mineral groups cluster about the origin. This finding suggests that the dust deposition process on the Huascarán col leads to a homogenous sorting of particles by size and shape, regardless of mineralogy. Mica deviates somewhat from this pattern in that the mineral grains are displaced towards slightly higher ECD values, but this observation is consistent with mica's large, flaky crystal habit. In general, these results, in conjunction with the negligible effect sizes for the morphological variables (main text; Section 4.4), indicate that mineralogy is a weak predictor of morphology.

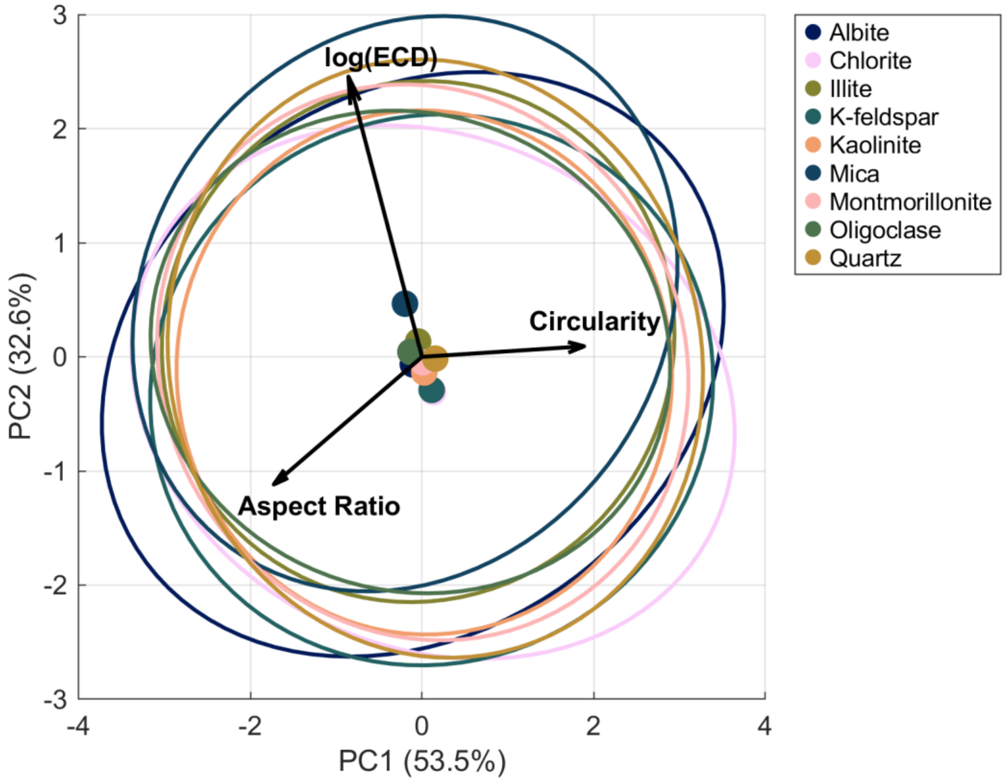

Figure S2. Biplot showing the morphological data in principal component space. Mineral centroids are plotted as scatter points along with 95% confidence ellipses.